




## REVIEW PAPER

Zuzanna Bober <sup>1(ABGF)</sup>, David Aebisher <sup>2(ABF)</sup>, Jacek Tabarkiewicz <sup>1,2(F)</sup>, Wiesław Guz <sup>1,3(F)</sup>,  
Piotr Tutka <sup>1,4(F)</sup>, Dorota Bartusik-Aebisher <sup>4(ABF)</sup>

# Investigation of pharmaceuticals by nuclear magnetic resonance imaging and spectroscopy

<sup>1</sup> Center for Innovative Research in Medical and Natural Sciences, Faculty of Medicine,  
University of Rzeszow, Rzeszow, Poland

<sup>2</sup> Department of Human Immunology, Faculty of Medicine, University of Rzeszow, Rzeszow, Poland

<sup>3</sup> Department of Electroradiology, Faculty of Medicine, University of Rzeszow, Rzeszow, Poland

<sup>4</sup> Department of Experimental and Clinical Pharmacology, Faculty of Medicine,  
University of Rzeszow, Rzeszow, Poland

## ABSTRACT

Currently, new and easier ways of analyzing pharmaceutical drug forms and drug delivery mechanisms are being sought. Magnetic resonance imaging (MRI) is a non-invasive imaging technique that images drug forms such as tablets, liquids and topicals and drug form behavior in living organisms on both the tissue and cellular scale. The advantages of MRI include non-invasiveness, variable sample capacity and ease of transfer of phantom results to *in vitro* and *in vivo* studies. This review concerns the usefulness of clinical MRI that cannot be understated as this technique provides non-invasive and non-destructive insight into the properties of drug delivery systems. The research discussed here concerns the use of magnetic resonance, spectroscopy and chromatography to investigate selected pharmaceuticals and covers work of selecting drugs and antibodies for modification by synthesis for evaluation by MRI. Modifications have been aimed at improving therapeutic efficacy, delivery, and MRI. Modification conditions such as (pH, concentration, temperature, and the influence of other components present in the solutions) will be discussed to understand drug delivery system improvements and the reliability and repeatability of the results obtained. We hope to explore and expand the scope of pharmaceutical imaging with MRI for application in clinical medicine.

**Keywords.** drug delivery systems, drug forms, magnetic resonance imaging, pharmaceuticals

---

**Corresponding author:** Dorota Bartusik-Aebisher, e-mail: [dbartusik-aebisher@ur.edu.pl](mailto:dbartusik-aebisher@ur.edu.pl)

**Participation of co-authors:** A – Author of the concept and objectives of paper; B – collection of data; C – implementation of research; D – elaborate, analysis and interpretation of data; E – statistical analysis; F – preparation of a manuscript; G – working out the literature; H – obtaining funds

Received: 16.01.2017 | Accepted: 18.04.2017

Publication date: June 2017

Bober Z, Aebisher D, Tabarkiewicz J, Guz W, Tutka P, Bartusik-Aebisher D. *Investigation of pharmaceuticals by nuclear magnetic resonance imaging and spectroscopy*. *Eur J Clin Exp Med*. 2017;15(2):110–119. doi: 10.15584/ejcem.2017.2.3

## Introduction

Currently one of the most accurate non-invasive imaging methods is magnetic resonance imaging (MRI). This method allows one to make sections in any plane of both living organisms and non-anatomical structures. The signals we receive in MR depend on the object being tested and its properties. We have the ability to obtain data with morphological, functional and metabolic information. To non-invasively monitor drugs inside the human body is a challenge. However, MRI has not been yet used in its full capacity in the field of pharmacy. The application of MRI in the sphere of pharmacy began in 1995 and is constantly developing. The main applications of MRI *in vitro* are monitoring of water and other solvents, controlled release of dosage forms, hydration and diffusion. The use of MRI in pharmacy can provide a platform to transfer knowledge from an *in vitro* study to an *in vivo* study in drug delivery and controlled release of dosage forms. This transfer of knowledge already takes place in research and there are several example studies on neurological drugs, anticancer drugs and vitamins. The first application of MRI in pharmacy to study pharmaceutical tablets was published by Nebgen et al. where the authors showed the distribution of porosity in tablets which is an important subject for the generation of solid drugs.<sup>1</sup> In another work published by Hyde *et al.*, the first quantitative MRI investigation based on a study of water migration from phosphate buffered solution into monolithic implants made of poly(glycolic acid-co-DL-lactic acid) produced by an extrusion process was conducted.<sup>2</sup> MRI is interesting for the magnetic properties of the nuclei of individual atoms. Each nuclei has its magnetic moment, which along with the applied magnetic field align with the lines of the field. The resulting weak net magnetization process when disturbed from equilibrium. The frequency of precession ( $\omega$ ) is equal to the applied magnetic field ( $B$ ) multiplied by the magnetogyric ratio ( $\gamma$ ). The magnetogyric ratio,  $\gamma$ , is a property that varies for different nuclei, being largest for the hydrogen nucleus  $\gamma=42,58 \text{ s}^{-1}\text{T}^{-1}$ . Radiowaves of angular frequency ( $\omega$ ) show a resonant interaction with the nuclei. A pulse of radio waves at this frequency can therefore be used to disturb the nuclei from equilibrium and set them into precession. Unfortunately, the MR signal is intrinsically weak, but increases in strength with increasing  $\gamma$  and  $B$ . MRI is therefore generally only applied to samples containing  $^1\text{H}$  nuclei in high concentrations. One MRI technique is magnetic resonance spectroscopy (MRS). MRS is a diagnostic tool used to characterize tissues in terms of their chemical composition.<sup>3-5</sup> MRS is used to determine the chemical properties of a given area, focusing on the metabolites of the cells. The method is based on the effect of the chemical shift of the atom (nuclei of different cells precess at different frequencies).<sup>6-7</sup> Most commonly performed experiment is single-voxel spectroscopy (SVS),

where the signal is received from the selected location. Measurements are made using PRESS (Pointed-Resolved Spectroscopy) or STEAM (Stimulated Echo Acquisition Mode) sequences. Based on the recorded signal from a given voxel, a Fourier transform is calculated and then spectra are generated on which individual peaks correspond to individual metabolites.<sup>8</sup> A chemical shift graph of signal frequency in parts-per-million (ppm) is generated from the signal amplitude. The area under the peak corresponds to the concentration of the metabolite. This provides the possibility of quantification of signal by using internal standards. Measurements are made using the PRESS (Pointed-Resolved Spectroscopy) or STEAM (Stimulated Echo Acquisition Mode) sequences. Based on the recorded signal from a given voxel, Fourier transform is calculated, and then spectra are generated on which individual peaks correspond to individual metabolites. In a technique called Magnetic Resonance Spectroscopic Imaging (MRSI), we can obtain color maps where the concentration level of a particular metabolite is encoded by color. Identification and quantification of the metabolite such as N-acetyl l-aspartic acid (2.02 ppm), creatine (3.02 ppm), choline (3.22 ppm) and lactate (1.33 ppm) in phantom were performed using SAGE post processing software. In order to evaluate the performance of an MR system, an MR phantom has been developed to accurately analyze errors of MR systems.<sup>9-11</sup> This makes it possible to visualize the distribution of metabolites throughout the brain. This is problematic, however, because the data received may include voxel bleeding, that is, voxel noise from the surrounding voxels.<sup>12-14</sup>

## MRI in pharmacy

The pharmaceutical sector has MRI related examples where formulations have been studied by observing tablet hydration and its effect during dissolution. MRI has been used to study internal mechanisms underlying *in vitro* drug release behavior in dosage forms, to monitor events within pharmaceutical processes, and *in vivo* to investigate the behavior of drug delivery systems in the body.<sup>15</sup> Examples of pre-clinical and *in vitro* MRI in new drug design studies include forms such as nanoparticles,<sup>16-20</sup> and nanogels.<sup>21</sup> Drug delivery systems use MRI to map drug transport and physiological response. Drug development<sup>22-23</sup> and drug release<sup>24-28</sup> have also been studied by MRI. As shown in the PubMed Data Base, the number of total publications regarding the applications of MRI in pharmacy is constantly increasing.

The authors provide innovative and creative examples of the use of MRI research in pharmacy. Also, the number of publications on contrast agents has increased due to intensive searches for improvement of diagnostic methods. With MRI, we are able to provide non-invasive ways to visualize events during controlled-release dosage. Using MRI, we also have a tool that is helpful in

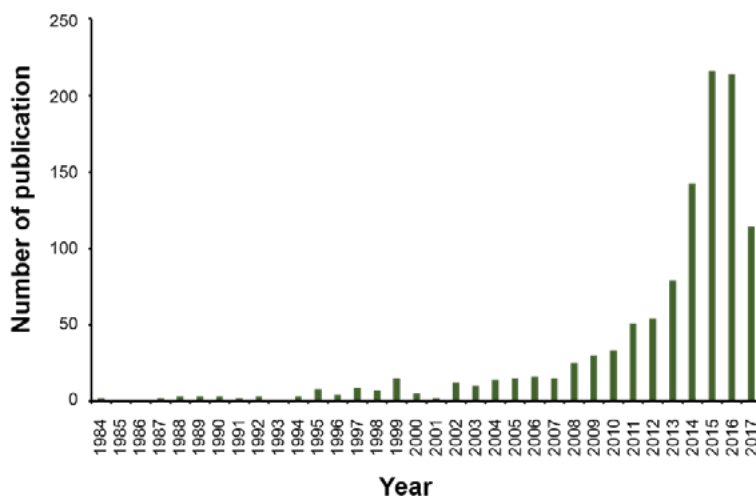


**Figure 1.** Publications on MRI Applications in Pharmacy

understanding the processes that occur in drug metabolism. This may have a significant impact on the development of a new generation of pharmaceuticals<sup>29</sup>. Porosity and compaction density are important parameters in the manufacture of tablets by compression. Nebgen *et al.* have shown how MRI can provide a noninvasive method for mapping the density distribution within a compacted tablet at a spatial resolution of (95  $\mu\text{m}$ ). However, factors such as paramagnetic materials, water–air, and solid–air interfaces can cause MRI artifacts.<sup>30–32</sup> MRI can identify tissue macromolecules such as nucleic acids, lipids, collagen and proteoglycans using parameters such as chemical shift, relaxation rates, and magnetic spin couplings. The enormous potential of MR to translation of the complex physical and mathematical concepts into biological material is recently an emerging area of empirical and theoretical interests. The MR techniques to determine proton relaxation times spin - lattice  $T_1$  and spin - spin  $T_2$  are numerous. These include a method fully relaxed Inversion recovery (IR)<sup>33</sup>, Fast Inversion Recovery (FIR)<sup>34</sup>,

Modified Fast Inversion Recovery (MFIR)<sup>35</sup>, Progressive Saturation (PS)<sup>36</sup>, Saturation Recovery (SR)<sup>37</sup>, Variable Nutation (VN)<sup>38</sup>, Look Locker (LL)<sup>39</sup>, choice of flip angles, delay intervals, and amount of signal averaging. These methods in a greater or lesser extent take advantage to provide a  $T_1$  and  $T_2$  measurements.<sup>40–41</sup>  $T_1$  and  $T_2$  in MRI are functions of spin density and also instrumental parameters such as the pulse sequence timing and slice selective sensitivity profile.<sup>42</sup> In liquids at higher temperatures  $T_1$  and  $T_2$  are almost equal. However, in solids and at low temperatures, there little molecular motion,  $T_1$  may be many seconds while  $T_2$  is only microseconds. The most commonly used methods in MRI for generating  $T_1$  maps are based on the basic pulse sequences used for  $T_1$  measurements in Nuclear Magnetic Resonance (NMR) spectroscopy: PS and IR. These radio-frequency pulse sequences can be combined with several imaging techniques and are used frequently in MRI.<sup>43</sup> The relaxation process is characterized by two exponential time constants  $T_1$  and  $T_2$ . The transient time-domain signal

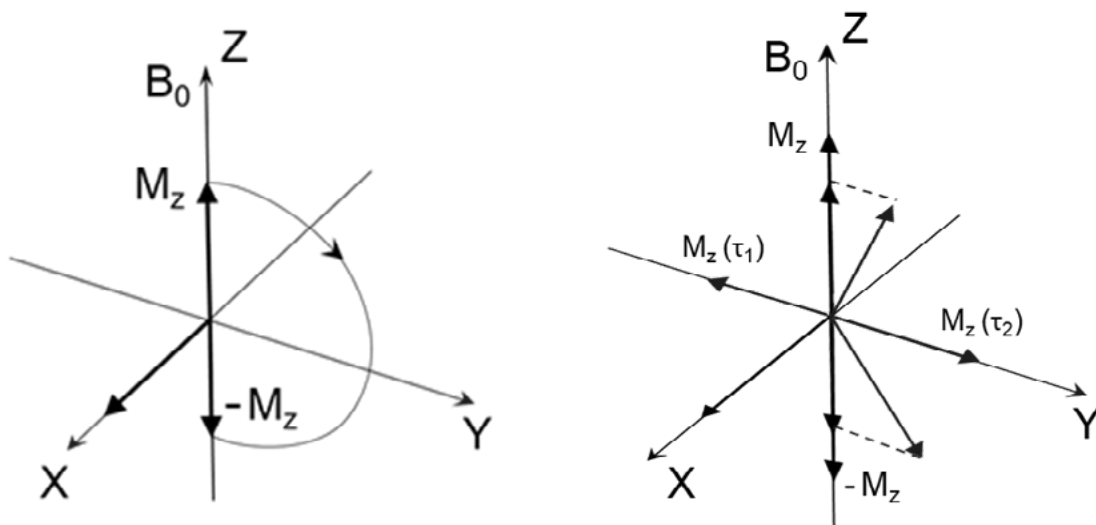


**Figure 2.** The MRI phenomenon

is digitized and stored in a computer. In MRI, the resultant magnetization aligned with the static magnetic field, which is called longitudinal magnetization, is tipped into the transverse plane, where it can be detected as an electric signal. This so-called transverse magnetization decays exponentially with a time constant  $T_2$ . The longitudinal magnetization relaxes back to its equilibrium orientation parallel to the static magnetic field exponentially with a time constant  $T_1$ . The mechanisms by which contrast agents enhance relaxation involve the magnetic moments. Relaxation does not occur spontaneously, it must be stimulated. Longitudinal magnetization relaxes toward equilibrium as excited spins undergo transitions to lower energy states.<sup>44</sup> These transitions must be stimulated by a changing magnetic field. A magnetic field oscillating in strength at the Larmor frequency supplies a quantum of energy exactly equal to the energy difference between the two states, thereby stimulating relaxation. The magnetic moments associated with particles such as nuclei, electrons, and atoms supply changing magnetic fields to stimulate relaxation (Figure 2). These magnetic field fluctuations are vital for relaxation.<sup>45</sup>

The first published calculated  $T_1$  image was generated in 1978 using sequence PS showed in Figure 3. Briefly, after the first 90 degree pulse, the magnetization is perturbed within the selected slice into the transverse plane. The transverse magnetization processes during the time interval TE and relaxes exponentially with a time constant as the 180 degree pulse refocuses any dephasing due to field in homogeneities. Longitudinal relaxation occurs during the interval TR until the next sequence repetition. If the next 90 degree pulse is applied the longitudinal magnetization has been allowed to recover completely during the intermediate period.<sup>46</sup>

Most MR studies indicated that the often used pulse sequence to measure  $T_1$  relaxation time is the IR measurements.<sup>40</sup> The pulse diagram for IR is shown in Figure 4. Briefly, 180 degree pulse inverts the magnetization vector MZ. After this the magnetization lies along the negative z axis and  $MZ = -M_0$ . The  $T_1$  relaxation makes the magnetization increase during time interval from  $-M_0$

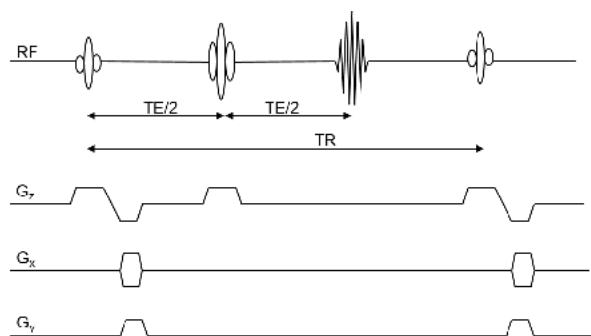


**Figure 3.** Partial or progressive saturation in a 2D Fourier Transform spin-echo pulse sequence

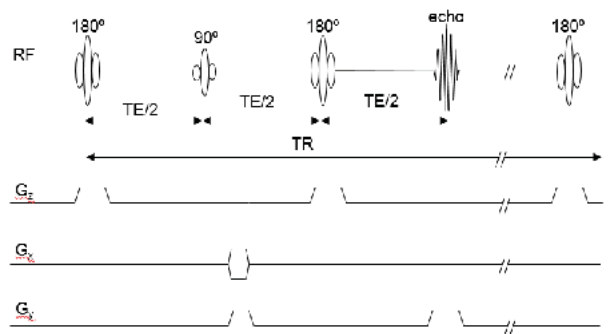


**Figure 4.** Inversion Recovery

throughout zero until it is back to original value  $MZ = M_0$ . If at some time following the 180 degree pulse, the 90 degree pulse is applied MZ is rotated around the X axis and will then lie somewhere along the Y axis. A  $T_1$  of a 90 degree pulse reads the relaxed magnetization.<sup>47</sup>

$T_1$  maps can also be generated by using a variable-tip-angle pulse during the MRI experiment. In this method, a pulse of tip angle zero-0 is used to perturb the magnetization, which is then left to partially relax back to its thermal equilibrium value during the short TR. As the excitation pulse is generally other than 90 degree only a fraction of the thermal equilibrium magnetization is tipped into the transverse plane. This transverse magnetization is then a function of both the pulse tip angle  $\theta$  and the amount of longitudinal relaxation that has occurred during the time interval TR.<sup>48</sup> In this case, the application of a 180 refocusing pulse to form a spin echo cannot be used, because such a pulse also would invert the magnetization that has remained along the longitudinal axis. Instead, an echo is formed through the use of gradients. This radio-frequency pulse sequence can then be incorporated into any imaging regime Figure 5. The transverse relaxation during TE is now described by the effective transverse relaxation time constant.<sup>49</sup>

Figure 5 presents a pulse sequence where  $T_1$  derives from the ratio of the STE of the SE and is formed from the first two pulses. Equation 1 shows the ratio of STE and SE where TM is the time between the second and third pulses.

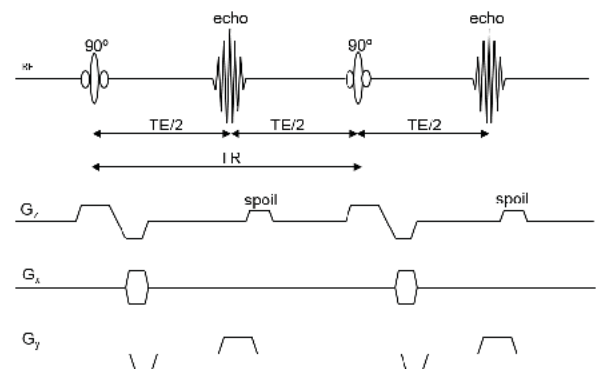


**Figure 5.** Variable tip angle, 2D Fourier transform gradient recalled echo pulse sequence

$$\text{STE}/\text{SE} = \exp(-\text{TM}/T_1)$$

This assumes perfect 90° pulses. Also to eliminate diffusion effects, a plot of  $1/T_{1\text{eff}}$  against TE2 yields a straight line whose intercept at TE = 0 is  $1/T_1 - T_{1\text{eff}}$  is the measured  $T_1$  at each TE.<sup>50</sup> A SE sequence in which the magnetization stored on the z axis during TM is sampled with a series of pulses with increasing flip angles designed to give equal SI in the absence of  $T_1$  relaxation.  $T_1$  is calculated from  $\text{SI} = S_0 \exp(\text{TM}/T_1)$ . Two pulses produce a SE, and a series of low-angle pulses then produce a series of STEs. The  $T_1$  is derived from the SE and STE intensities, which would all be the same if there were no  $T_1$  relaxation. SE is very sensitive to flip-angle errors and could be improved by the SNR by changing the flip angle of the second pulse to 180 degree. It was found that a composite echo with a SE and a STE 90 degree out of phase and calculated  $T_1$  from the phase of the signal. Phantom STE data are similar to IR data, but human STE data were not compared to IR phantom data (Figure 6-7).<sup>51</sup>

MRI and MRS measurements show that engineered liposomes can detect the mildly acidic pH of the tumor microenvironment with 0.2 pH unit precision and they release their content into C6 glioma tumors selectively, *in vivo*.<sup>52</sup> MRSI of the pH sensitive probe (+/-)-2-(imidazol-1-yl)succinic acid disodium salt and a pH map of a tumor *in vivo* was investigated. Citrate, choline-containing compounds, creatine and polyamines have also been described by MRSI. The protons of Citrate resonate around 2.6 ppm, but the precise chemical shift and the scalar coupling of these protons depend on pH and cation concentration in cellular membranes.<sup>53</sup> MRSI was used in neurooncology but also in multiple sclerosis, stroke and epilepsy. However, a major challenge in conventional MRSI is the longer acquisition time required for adequate signal to be collected.<sup>54</sup>

Studies to characterize the reliability of MRSI thermometry, including contributions from inter-scan and interexamination variability have been performed. In addition, measurements of the variation between subjects and assessment of the extent of brain temperature variation.<sup>55</sup> MRSI also provides spatially localized maps of metabolite concentrations.<sup>56</sup> MRSI provides a unique modality to non-invasively study tissue metabolism *in vivo*; it acquires metabolic information reflecting tissue function and provides a sensitive assessment of chemical alterations.<sup>57</sup> Table 1-3 presents the applications of MRI to study the forms of drugs and properties.

The study provided by Zeitler and co-worker showed as a calibration set such that the MRI signal from the pore space of the tablet could provide a measure of tablet density. Different sets of production tablets were analyzed using the MRI method and the density distribution within the dosage form was determined.<sup>76</sup> Since  $T_1$  of pure water can be 3–5 s and the image acquisition

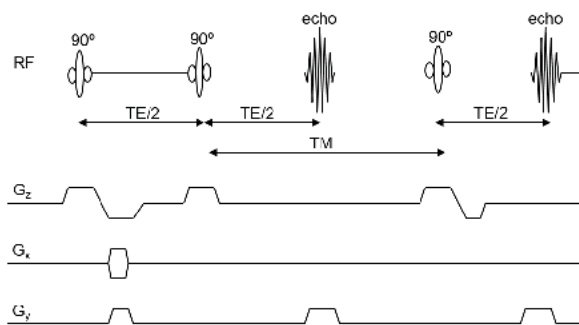


Figure 6. STE sequence

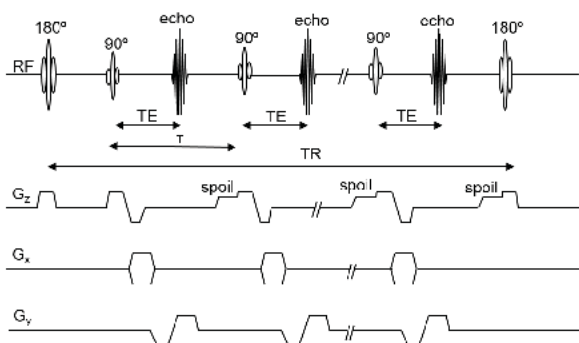


Figure 7. Multiple gradient echo

time is proportional to TR, this can lead to poor temporal resolution. In addition, the shortest achievable TE is restricted by the finite time required to turn the gradients on and off, limited by the hardware, as well as the time to record the signal. The use of low-field MRI (typically 0.5 Tesla) for pharmaceutical research, and specifically for tablet dissolution, has been limited partly due to the availability of instrumentation and also the perceived lack of sensitivity.<sup>77</sup> Nickel-doped agarose/sucrose gels can be used as reference materials for MRI diffusion measurements and show excellent short-term stability with respect to ADC. A phantom made of these materials can be invaluable in optimizing DW-MRI protocols, developing novel pulse sequences for DW-MRI, or comparing ADC values among field strengths, vendors, and imaging centers.<sup>78</sup> Magnetic Block Ionomer Clusters with hydrophilic ionic cores and nonionic coronas have been prepared that have ultrahigh transverse NMR relaxivities together with capacities for incorporating high concentrations of polar antibiotic payloads. Magnetite-polymer nanoparticles were assembled by adsorbing the polyacrylate block of an aminofunctional poly(ethylene oxide-*b*-acrylate) (H2N-PEO-*b*-PAA) copolymer onto magnetite nanoparticles.<sup>79</sup> Magnetic nanoparticles possess unique magnetic properties and the ability to function at the cellular and molecular level of biological interactions making them an attractive platform as contrast agents for MRI and as carriers for drug delivery. Recent advances in nanotechnology have

**Table 1.** MRI in Pharmacy

Authors	Ref	Sample	Experiment
Nebgen G et al.	31	circular tablet	qualitative study on the hydration of HPMC tablets
Soussi B. et al.	58	implant	extruded monolithic zero-order release kinetics implant; characterization of the liquid in polymer by $T_2$ maps
Hyde T. and Gladden L.	59	circular tablet	qualitative imaging study of the erosion of the drug containing compartment of a dry coated controlled release tablet
Peppas N. et al.	60	extrudate	measurement of water distribution in lipid/MCC extrudates processed at different speed and different water content in the formulation
Fyfe C. and Blazek-Welsh A.	32	spherical pellet	drug release from different formulations of API loaded lipid matrix pellets; diffusion measurements using PGSE sequence
Harding S. et al.	61	lipophilic matrix heophylline beads	quantitative imaging experiment of the liquid concentration, $T_2$ distribution and self-diffusion coefficient within poly(glycolic lactic acid) controlled release drug delivery system
Malveau C. et al.	62	capsule plug	dissolution study of coated pulsatile release capsules; release is triggered by swelling hydrogel plug
Johns M. and Gladden L.	63	circular tablet	quantitative measurement of the polymer concentration during the hydration of tablets
Baumgartner S. et al.	64	circular tablet	swelling and water diffusion was studied in samples of high amylose starch tablets
Richardson JC et al.	15	circular tablet	porosity imaging of tablets penetrated by gadolinium-doped silicon oil
Djemai A and Sinka I.	65	circular tablet	water penetration into the tablets is studied experimentally
Karakosta E. and McDonald P.	66	spherical pellet	pore structure evolution in pellets during dissolution; pellets were made of lactose and MCC
Marchessault R. et al.	67	circular tablet	porosity measurement of tablets made of three different excipients (MCC, lactose and anhydrous calcium phosphate) compressed at different pressures
Mäder K. et al.	68	capsule plug	dissolution study of capsules formulated from HPMC and L-dopa using flow through cell in a horizontal magnet

**Table 2.** MRI measurements of drugs

MRI drugs	
Maximum sample size	5 mm to 30 cm
Measurement possibilities	chemical specificity to nuclei of interest (intrinsic signal) nuclear spin relaxation times molecular mobility
Chemical sensitivity	high
Advantages	chemical specificity in situ dissolution studies are possible quantitative technique ability to study flow and diffusion processes wide range of imaging sequences is available to specifically emphasise certain properties of the sample
Limitations	only some solids can be imaged directly the experiments are usually destructive as they require the interaction of a liquid phase with the sample operation of strong magnetic fields requires special safety precautions restricted sample size in magnetic more paramagnetic materials (such as most metals) have to be eliminated from the sample setup

**Table 3.**  $T_1$  and  $T_2$  times measurements *in vitro*

MRI of samples; $T_1$ and $T_2$ times measurements <i>in vitro</i>		
Author / [Ref]	Sample	Relaxation times
Haas A. / <sup>69</sup>	phantom containing: six tubes filled with water, doped with different concentrations of Gd(DTPA)	$T_1$ values varied from 140 ms up to 2400 ms
Aboagye E. <i>et al.</i> / <sup>60</sup>	phantom containing: (BT) background tissue compartment; (P1) and (P2) pathological tissues compartments; (OF) fat compartment; (A) air compartment	$T_1 = 1093$ ms, $T_2 = 91$ ms for P1; $T_1 = 993$ ms, $T_2 = 88$ ms for P2; $T_1 = 657$ ms, $T_2 = 84$ ms for BT
Keenan K. <i>et al.</i> / <sup>70</sup>	phantom: $\text{NiCl}_2$ solutions with varying concentration (0.3 mM to 69.68 mM), and $\text{MnCl}_2$ solutions with varying concentration (0.013 mM to 1.704 mM)	$T_1$ value of 2033-22 ms and $T_2$ value of 1669-20 ms for $\text{NiCl}_2$ ; $T_1$ value of 2376-83 ms and $T_2$ value of 939-8 ms for $\text{MnCl}_2$
Hiraki Y. <i>et al.</i> / <sup>71</sup>	phantom: $\text{GdCl}_3$ concentration was varied from 0–140 $\mu\text{mol/kg}$ and the agarose concentration was varied from 0–1.6% in a fixed carrageenan concentration of 3%	$T_1$ value of 202–1904 ms and $T_2$ value of 38–423 ms
Kato <i>et al.</i> / <sup>72</sup>	CAGN phantom containing: carrageenan, $\text{GdCl}_3$ , agarose, NaCl, $\text{NaN}_3$ and distilled water	$T_1$ values of 202–1904 ms and $T_2$ values of 38–423 ms when the concentrations of $\text{GdCl}_3$ and agarose are varied from 0–140 $\mu\text{mol/kg}$ , and 0%–1.6%
Jensen M., Caruthers S., Jara H. / <sup>73</sup>	phantom composed of several fluid-filled containers; phantom contains materials spanning the $T_1$ and $T_2$ relaxation times of the biologic range; (dilutions of gadolinium, distilled water, dilutions of ultrasound gel, corn oil, isopropyl alcohol, dilutions of glycerol, dilution of copper sulfate)	accurate $T_1$ measurements within the biologic range; $T_2$ measurements are accurate for $T_2$ values of less than about 500 ms, thus covering all known gel-like biologic tissues
Wickline S. <i>et al.</i> / <sup>74</sup>	phantom with highly potent paramagnetic liquid perfluorocarbon nanoparticle contrast agent (minimum concentration needed for diagnostic contrast)	input parameters: $T_1$ value of 1120 ms and $T_2$ value of 100 ms
Adriaensen H. <i>et al.</i> / <sup>75</sup>	four paramagnetic nickel sulfate ( $\text{NiSO}_4$ ) aqueous solutions with different relaxation times, and fruit (apple, tomato)	$T_2$ values of 26-1248 ms for $\text{NiSO}_4$ solutions; $T_2$ values of 53-506 ms for apple and $T_2$ values of 114-835 ms for tomato

improved the ability to specifically tailor the features and properties of MNPs for these biomedical applications.<sup>80</sup> The objective of this study was to prepare and characterize magnetic nanoparticles embedded in poly-lactide-co-glycolide matrixes (PLGA-MNPs) as a dual drug delivery and imaging system capable of encapsulating both hydrophilic and hydrophobic drugs. Magnetic resonance imaging was carried out both *in vitro* and *in vivo* to assess the efficacy of PLGA-MNPs as contrast agents. PLGA-MNPs showed a better contrast effect than commercial contrast agents due to higher  $T_2$  relaxivity with a blood circulation half-life~47 min in the rat model.<sup>81</sup> The inverse relationship between  $T_1$  and nanoparticle concentration accounts for the nonlinear increase in contrast, resulting in a modest leveling of the contrast effect at high concentrations when TE is kept to a minimum (~7 nM). The close agreement between the model and the phantom data supports extrapolations to lower concentrations of nanoparticles. If a CNR  $\geq 5$  is defined as the minimum diagnostically meaningful contrast, the model shows that only picomolar concentrations of nanoparticles need be present within a typically-sized imaging voxel to produce diagnostic contrast enhancement for molecular imaging.<sup>74</sup>

## Conclusion

The number of papers regarding the applications of MRI in pharmacy shows a huge progress in MRI hardware and software applied to biomedical research.

## References

1. Nebgen G, Gross D, Lehmann V, Muller F. <sup>1</sup>H NMR microscopy of tablets. *J Pharm Sci.* 1995;84:283-91.
2. Hyde T, Gladden L, Payne R. A nuclear-magnetic-resonance imaging study of the effect of incorporating a macromolecular drug in poly(glycolic acid-co-DL-lactic acid). *J Control Release.* 1995;36:261-75.
3. Lee P, Adany P, Choi IY. Imaging based magnetic resonance spectroscopy (MRS) localization for quantitative neurochemical analysis and cerebral metabolism studies. *Anal Biochem.* 2017;529:40-7.
4. Cudalbu C, Cooper AJL. Editorial for the special issue on introduction to *in vivo* Magnetic Resonance Spectroscopy (MRS): A method to non-invasively study metabolism. *Anal Biochem.* 2017;529:1-3.
5. Capati A, Ijare OB, Bezabeh T. Diagnostic Applications of Nuclear Magnetic Resonance–Based Urinary Metabolomics. *Magn Res Insights.* 2017;10:1.



6. Gillinder L, Yi GS, Cowin G, et al. Quantification of intramyocardial metabolites by proton magnetic resonance spectroscopy. *Front Cardiovasc Med.* 2015;2:24.
7. Mandal P, Shukla D, Govind V, Boulard Y, Erslund L. Glutathione Conformations and Its Implications for *in vivo* Magnetic Resonance Spectroscopy. *J Alzh Dis.* 2017;10.3233/JAD-170350.
8. Zhang Y, An L, Shen J. Fast Computation of Full Density Matrix of Multispin Systems for Spatially Localized *In Vivo* Magnetic Resonance Spectroscopy. *Med Phys J.* 2017;10.1002/mp.12375.
9. Sheikh ASE, Mohamed M. Magnetic resonance spectroscopy and magnetic resonance spectroscopic imaging in Cerebral Autosomal-Dominant Arteriopathy with Subcortical Infarcts and Leukoencephalopathy: A literature review. *J Pak Med Assoc.* 2017;67:912-16.
10. Younisa S, Hougaard A, Vestergaard M, Larsson H, Ashinaa M. Migraine and magnetic resonance spectroscopy: a systematic review. *Curr Opin Neur J.* 2017;30:246.
11. Guo L, Wang D, Bo G, Zhang H, Tao W, Shi Y. Early identification of hypoxic-ischemic encephalopathy by combination of magnetic resonance (MR) imaging and proton MR spectroscopy. *Exp Therap Med J.* 2016;12:2835-42.
12. Bertholdo D, Watcharakorn A, Castillo M. Brain proton magnetic resonance spectroscopy: introduction and overview. *Neuroimag Clin N Am.* 2013;23:359-80.
13. Soares DP, Law M. Magnetic resonance spectroscopy of the brain: review of metabolites and clinical applications. *Clin Radiol.* 2009;64:12-21.
14. Pagani E, Bizzi A, Di Salle F, De Stefano N, Filippi M. Basic concepts of advanced MRI techniques. *Neurol Sci.* 2008;29,3:290-5.
15. Richardson JC, Bowtell R, Mäder K, Melia C. Pharmaceutical applications of magnetic resonance imaging (MRI). *Adv Drug Deliv Rev.* 2005;57:1191.
16. Figueiredo P, Lintinen K, Kiriazis A, et al. *In vitro* evaluation of biodegradable lignin-based nanoparticles for drug delivery and enhanced antiproliferation effect in cancer cells. *Biomaterials.* 2017;121:97-108.
17. Sua X, Chana C, Shia J, et al. A graphene quantum dot@Fe<sub>3</sub>O<sub>4</sub>@SiO<sub>2</sub> based nanoprobe for drug delivery sensing and dual-modal fluorescence and MRI imaging in cancer cells. *Biosens Bioelectron.* 2017;92:489-95.
18. Feng Q, Zhang Y, Zhang W, et al. Programmed near-infrared light-responsive drug delivery system for combined magnetic tumor-targeting magnetic resonance imaging and chemo-phototherapy. *Acta Biomater.* 2017;49:402-13.
19. Banoa S, Afzal M, Waraich M, Alamgire K, Nazir S. Paclitaxel loaded magnetic nanocomposites with folate modified chitosan/carboxymethyl surface; a vehicle for imaging and targeted drug delivery. *Intern J Pharm.* 2016;513:554-63.
20. Chen Y, Ai K, Liu J, Sun G, Yin Q, Lu L. Multifunctional envelope-type mesoporous silica nanoparticles for pH-responsive drug delivery and magnetic resonance imaging. *Biomaterials.* 2015;60:111-20.
21. Ma Y, Ge Y, Li L. Advancement of multifunctional hybrid nanogel systems: Construction and application in drug co-delivery and imaging technique. *Mat Sci Eng.* 2017;71:1281-92.
22. Raggi P, Baldassarre D, Day S, de Groot E, Fayad ZA. Non-invasive imaging of atherosclerosis regression with magnetic resonance to guide drug development. *Atherosclerosis.* 2016;251:476-82.
23. Lin B, Su H, Jin R, Li D, Wu C, Jiang X, Xia C, Gong Q, Song B, Ai H. Multifunctional dextran micelles as drug delivery carriers and magnetic resonance imaging probes. *Sci Bull.* 2015;60:1272.
24. Punčochová K, Ewing AV, Gajdošová M, et al. Identifying the mechanisms of drug release from amorphous solid dispersions using MRI and ATR-FTIR spectroscopic imaging. *Intern J Pharm.* 2015;483:256.
25. Um SY, Par JH, Chung MW, Choic KH, Lee HJ. <sup>1</sup>H-Nuclear magnetic resonance-based metabolic profiling of nonsteroidal anti-inflammatory drug-induced adverse effects in rats. *J Pharm Biomed Anal.* 2016;129:492-501.
26. Pacheco-Torres J, Mukherjee N, Walko M, et al. Image guided drug release from pH-sensitive Ion channel-functionalized stealth liposomes into an *in vivo* glioblastoma model. *Nanomed: Nanotech Biol Med.* 2015;11:1345-54.
27. Li L, Zhang R, Guo Y, et al. Functional magnetic porous silica for T<sub>1</sub>-T<sub>2</sub> dual-modal magnetic resonance imaging and pH-responsive drug delivery of basic drugs. *Nanotech.* 2016;27:485702.
28. Gao N, Bozeman E, Qian W, et al. Tumor Penetrating Theranostic Nanoparticles for Enhancement of Targeted and Image-guided Drug Delivery into Peritoneal tumors following Intraperitoneal Delivery. *Theranostics.* 2017;7:1689-94.
29. Melia CD, Rajabi-Siahboomi A, Bowtell R. Magnetic resonance imaging of controlled release pharmaceutical dosage forms. *Pharm Sci & Techn Today.* 1998;1:32-5.
30. Bowtell R, Sharp J, Peters A, et al. NMR microscopy of hydrating hydrophilic matrix pharmaceutical tablets. *Magn Reson Imag.* 1994;12:361-4.
31. Tung NT, Tran CS, Nguyen TL, Hoang T, Trinh TD, Nguyen TN. Formulation and biopharmaceutical evaluation of bitter taste masking microparticles containing azithromycin loaded in dispersible tablets. *Eur J Pharm Biopharm* 2017; doi: 10.1016/j.ejpb.2017.03.017
32. Fyfe CA, Blazek A. Investigation of hydrogel formation from hydroxypropylmethylcellulose (HPMC) by NMR spectroscopy and NMR imaging techniques. *Macromolecules.* 1997;30:6230.
33. Wang X, Roeloffs V, Kłosowski J, et al. Model-based T<sub>1</sub> mapping with sparsity constraints using single-shot inversion-recovery radial FLASH. *Magn Reson Med.* 2017; DOI: 10.1002/mrm.26726.
34. Mazumdar A, Siegel MJ, Narra V, Luchtman-Jones L. Whole-Body Fast Inversion Recovery MR Imaging of Small Cell Neoplasms in Pediatric Patients: A Pilot Study. *Am J Roentgen.* 2002;179:1261-126.



35. Gupta RK. A modified fast inversion-recovery technique for spin-lattice relaxation measurements. *J Magn Reson.* 1980;38:447-452.
36. Helms G, Hagberg GE. *In vivo* quantification of the bound pool  $T_1$  in human white matter using the binary spin-bath model of progressive magnetization transfer saturation. *Phys Med & Biol.* 2009;54:23-25.
37. Chow K, Flewitt JA, Green JD, Pagano JJ, Friedrich MG, Thompson RB. Saturation recovery single-shot acquisition (SASHA) for myocardial  $T_1$  mapping. *Magn Reson Med.* 2013;71:2082-95.
38. Deoni SCL, Peters TM, Rutt BK. Determination of optimal angles for variable nutation proton magnetic spin-lattice,  $T_1$ , and spin-spin,  $T_2$ , relaxation times measurement. *Magn Reson Med.* 2003;51:194-9.
39. Messroghli DR, Nordmeyer S, Dietrich T, et al. Assessment of Diffuse Myocardial Fibrosis in Rats Using Small-Animal Look-Locker Inversion Recovery  $T_1$  Mapping. *Cardiovasc Imag.* 2011;4:636-40.
40. Träber F, Block W, Lamerichs R, Gieseke J, Schild HH.  $^1\text{H}$  metabolite relaxation times at 3.0 tesla: Measurements of  $T_1$  and  $T_2$  values in normal brain and determination of regional differences in transverse relaxation. *J Magn Reson Imag.* 2004;19:537-45.
41. Mlynárik V, Gruber S, Moser E. Proton  $T_1$  and  $T_2$  relaxation times of human brain metabolites at 3 Tesla. *NMR in Biomed.* 2001;14:325-31.
42. Bouhrara M, Bonny JM.  $B_1$  mapping with selective pulses. *Magn Reson Med.* 2012;68:1472-80.
43. Dai W, Garcia D, de Bazelaire C, Alsop DC. Continuous flow-driven inversion for arterial spin labeling using pulsed radio frequency and gradient fields. *Magn Reson Med* 2008;60:1488-97.
44. Gelman N, Ewing JR, Gorell JM, Spickler EM, Salomon EG. Interregional variation of longitudinal relaxation rates in human brain at 3.0 T: Relation to estimated iron and water contents. *Magn Reson Med.* 2001;45:71-9.
45. Kiessling F, Pichler BJ. *Small Animal Imaging: Basics and Practical Guide.* Springer Science & Business Media. 2010;150-5.
46. Shah B, Anderson SW, Scalera J, Jara H, Soto JA. *Quantitative MR Imaging: Physical Principles and Sequence Design in Abdominal Imaging.* RadioGraphics. 2010;31:867-80.
47. Huang J, Zhang M, Lu J, Cai C, Chen L, Cai S. A fast chemical exchange saturation transfer imaging scheme based on single-shot spatiotemporal encoding. *Magn Reson Med.* 2017;77:1786-96.
48. Bydder GM, Pennock JM, Steiner RE, Khenia S, Payne JA, Young IR. The short TI inversion recovery sequence--an approach to MR imaging of the abdomen. *Magn Reson Imaging.* 1985;3:251-4.
49. Kurland RJ. Strategies and tactics in NMR imaging relaxation time measurements. I. Minimizing relaxation time errors due to image noise--the ideal case. *Magn Reson Med.* 1985; 2:136-58.
50. Bydder GM, Pennock JM, Steiner RE, Khenia S, Payne JA, Young IR. The short TI inversion recovery sequence--an approach to MR imaging of the abdomen. *Magn Reson Imaging.* 1985;3:251-4.
51. Hardy CJ, Edelstein WA, Vatis D, Harms R, Adams WJ. Calculated T1 images derived from a partial saturation-inversion recovery pulse sequence with adiabatic fast passage. *Magn Reson Imaging.* 1985;3:107-16.
52. Pacheco-Torres J, Mukherjee N, Walko M, et al. Image guided drug release from pH-sensitive Ion channel-functionalized stealth liposomes into an *in vivo* glioblastoma model. *Nanomedicine.* 2015;11:1345-54.
53. Tayari N, Heerschap A, Scheenen TWJ, Kobus T. *In vivo* MR spectroscopic imaging of the prostate, from application to interpretation. *Anal Biochem.* 2017;529:158-70.
54. Al-Iedani O, Lechner-Scott J, Ribbons K, Ramadan S. Fast magnetic resonance spectroscopic imaging techniques in human brain- applications in multiple sclerosis. *J Biomed Sci.* 2017;24:17-20.
55. Thrippleton MJ, Parikh J, Harris BA, et al. Reliability of MRSI brain temperature mapping at 1.5 and 3 T. *NMR in Biomedicine.* 2013;27:183-90.
56. Kasten J, Lazeyras F, Van De Ville D. Data-driven MRSI spectral localization via low-rank component analysis. *IEEE Trans Med Imaging.* 2013;32:1853-63.
57. Fu Y, Serrai H. Fast magnetic resonance spectroscopic imaging (MRSI) using wavelet encoding and parallel imaging: *in vitro* results. *J Magn Reson.* 2011;211:45-51.
58. Madhu B, Hjartstam J, Soussi B. Studies of the internal flow process in polymers by H NMR microscopy at 500 MHz. *J ControlRelease.* 1998;56:95-04.
59. Hyde T, Gladden L. Simultaneous measurement of water and polymer concentration profiles during swelling of poly(ethylene oxide) using magnetic resonance imaging. *Polymer.* 1998;4:811-9.
60. Narasimhan B, Snaar J, Bowtell R, Morgan S, Melia C, Pappas N. Magnetic Resonance Imaging Analysis of Molecular Mobility during Dissolution of Poly(vinyl alcohol) in Water. *Macromolecules.* 1999;32:704-10.
61. Harding S, Baumann H, Gren T, Seo A. NMR microscopy of the uptake, distribution and mobility of dissolution media in small, sub-millimetre drug delivery systems. *J Control Release.* 2000;66:81-99.
62. Malveau C, Baille W, Zhu X, Marchessault R. NMR imaging of high-amylose starch tablets. 2. Effect of tablet size. *Biomacromolecules.* 2002;3:1249-54.
63. Johns M, Gladden L. Magnetic resonance studies of dissolving particulate solids. *Magn Reson Imag.* 2003; 21: 395-6.
64. Baumgartner S, Lahajnar G, Sepe A, Kristl J. Quantitative evaluation of polymer concentration profile during swelling of hydrophilic matrix tablets using  $^1\text{H}$  NMR and MRI methods. *Eur J Pharm Biopharm.* 2005;59:299-06.
65. Djemai A, Sinka I. NMR imaging of density distributions in tablets. *Intern J Pharm.* 2006;319:55-62.

66. Karakosta E, McDonald P. An MRI analysis of the dissolution of a soluble drug incorporated within an insoluble polymer tablet. *Appl Magn Reson*. 2007;32:75–91.
67. Therien-Aubin H, Zhu X, Ravenelle F, Marchessault R. Membrane formation and drug loading effects in high amylose starch tablets studied by NMR imaging. *Biomacromolecules*. 2008;9:1248–54.
68. Strübing S, Abboud T, Contri R, Metz H, Mäder K. New insights on poly(vinyl acetate)-based coated floating tablets: Characterisation of hydration and CO<sub>2</sub> generation by benchtop MRI and its relation to drug release and floating strength. *Eur. J. Pharm. Biopharm*. 2008;69:708–17.
69. Haas A. Snapshot FLASH MRI. Applications to T<sub>1</sub>, T<sub>2</sub> and Chemical-Shift Imaging. *Magn Reson Med*. 1990;13:77–89.
70. Keenan K, Stupic K, Boss M, et al. Multi-site, multi-vendor comparison of T<sub>1</sub> measurement using ISMRM/NIST system phantom. *ISMRM 24th Annual Meeting*. 2016;55:3290.
71. Yoshimura K, Kato H, Kuroda M, et al. Development of a Tissue-Equivalent MRI Phantom Using Carrageenan Gel. *Magn Reson Med*. 2003;50:1011–17.
72. Kato H, Kuroda M, Yoshimura K, et al. Composition of MRI phantom equivalent to human tissues. *Am Assoc Phys Med*. 2005; DOI: 10.1118/1.2047807.
73. Jensen M, Caruthers S, Jara H. Quantitative Magnetic Resonance Imaging With The Mixed Turbo Spin-echo Pulse Sequence: A Validation Study. *The Internet J Radiol*. 2000;2(1).
74. Morawski AM, Winter PM, Crowder KC, et al. Targeted nanoparticles for quantitative imaging of sparse molecular epitopes with MRI. *Magn Reson Med*. 2004;51:480–6.
75. Adriaensen H, Musse M, Quellec S, Vignaud A, Cambert M, Mariette F. MSE-MRI sequence optimisation for measurement of bi- and tri-exponential T<sub>2</sub> relaxation in a phantom and fruit. *Magn Reson Imag*. 2013;31:1677–89.
76. Zeitler JA, Gladden LF. *In-vitro* tomography and non-destructive imaging at depth of pharmaceutical solid dosage forms. *Eur J of Pharm Biopharm*. 2009;71:2–22.
77. Nott KP. Magnetic resonance imaging of tablet dissolution. *Eur J Pharm Biopharm* 2010;74:78–83.
78. Lavdas I, Behan KC, Papadaki A, McRobbie DW, Aboagye EO. A phantom for diffusion-weighted MRI (DW-MRI). *J Magn Reson Imag*. 2013;38:173–9.
79. Pothayee N, Balasubramaniam S, Pothayee N, et al. Magnetic Nanoclusters with Hydrophilic Spacing for Dual Drug Delivery and Sensitive Magnetic Resonance Imaging. *J Mater Chem B Mater Biol Med*. 2013;1:1142–9.
80. Jain TK, Richey J, Strand M, Leslie-Pelecky DL, Flask C, Labhasetwar V. Magnetic Nanoparticles with Dual Functional Properties: Drug Delivery and Magn Reson Imag *Biomater* 2008;29:4012–21.
81. Singh A, Dilnawaz F, Mewar S, Sharma U, Jagannathan NR, Sahoo SK. Composite Polymeric Magnetic Nanoparticles for Co-Delivery of Hydrophobic and Hydrophilic Anticancer Drugs and MRI Imaging for Cancer Therapy. *ACS Appl Mater Interfaces*. 2011;3:842–56.